Eur Radiol (2005) 15: 653–660
DOI 10.1007/s00330-004-2547-2



**Matthias P. Lichy**
**Jörg Pintaske**
**Raimund Kottke**
**Jürgen Machann**
**Aristotelis Anastasiadis**
**Stefan Roell**
**Jörg Hennenlotter**
**Till Diergarten**
**Fritz Schick**
**Arnulf Stenzl**
**Claus D. Claussen**
**Heinz-Peter Schlemmer**

# 3D proton MR spectroscopic imaging of prostate cancer using a standard spine coil at 1.5 T in clinical routine: a feasibility study

Received: 5 May 2004
Accepted: 7 October 2004
Published online: 31 December 2004


M. P. Lichy · J. Pintaske · R. Kottke · J. Machann · T. Diergarten · F. Schick · C. D. Claussen · H.-P. Schlemmer
Department of Radiologic Diagnostics, Eberhard-Karls University Tuebingen, 72076 Tuebingen, Germany

M. P. Lichy (✉) · J. Pintaske · J. Machann · F. Schick
Section on Experimental Radiology, Eberhard-Karls University Tuebingen, 72076 Tuebingen, Germany
e-mail: matthias.lichy@med.uni-tuebingen.de
Tel.: +49-7071-2980546

A. Anastasiadis · J. Hennenlotter · A. Stenzl
Department of Urology, Eberhard-Karls University Tuebingen, 72076 Tubingen, Germany

S. Roell
Siemens AG, Medical Solutions MR Application Development, Spectroscopy (MREA-MRS), 91050 Erlangen, Germany

**Abstract** The objective of this study was to demonstrate the feasibility of 3D proton MR spectroscopic imaging (MRSI) of the prostate using a standard spine instead of a dedicated endorectal coil at 1.5 T. Twenty-eight patients (25 with biopsy proven prostate cancers and three patients with a benign prostate hyperplasia) were examined. MRI and MRSI were conducted with commercial array surface coils at 1.5 T. Ratios of choline (Cho), creatine (Cr) and citrate (Ci) were calculated for tumour, central and peripheral zone retrospectively, based on axial T2 weighed MR images and histology reports. Prostate cancer was characterized by significantly elevated (Cho+Cr)/Ci ratio compared with non-tumourous prostate tissue. The quality of all proton MR spectra was considered to be good or acceptable in 17/28 patients (61%) and poor in 11/28 (39%) examinations. In 20/25 patients with proven malignancy (80%), MRSI was considered to be helpful for the detection of prostate cancer. In 4/25 patients with proven malignancy (16%) who underwent seed implantation, radiotherapy or hormone deprivation before MR examination spectroscopy was of poor and non-diagnostic quality. MRSI of the prostate is feasible within clinical routine using the spine array surface coil at 1.5 T. It can consequently be applied to patients even with contraindications for endorectal coils. However, spectral quality and signal-to-noise ratio is clearly inferior to 3D MRSI examinations with endorectal coils.

**Keywords** MR spectroscopy · Prostate · Cancer

## Introduction

Prostate cancer is the most common non-skin related malignancy in men of industrialised countries [1], affecting about one out of 11 males. After lung cancer, prostate cancer has the second highest mortality rate in western countries. Although prostate cancer is typically diagnosed in older men, younger individuals (<50 years of age) can also be affected.

Early prostate cancer detection has been significantly improved by serum testing for prostate specific antigen (PSA). However, diagnosis has to be verified by ultrasound-guided biopsy, since elevated PSA serum levels can also be caused by benign conditions, such as benign prostatic hyperplasia (BPH), which is also prevalent in older men.

Treatment strategies for prostate cancer include radical prostatectomy, external radiotherapy, iodine-seed brachytherapy, hormonal therapy and “watchful waiting”.

Individual treatment planning and "watchful waiting" [2] requires accurate diagnostic tools for tumour localization and staging. At present, however, MRI performed with endorectal coil is unsuitable as a primary diagnostic tool for detecting prostate cancer due to its low specificity and low positive predictive value [3]. Signal changes of T2-weighted MR images are uncharacteristic and can also be caused by inflammation or benign prostatic hyperplasia. However, after histopathologic confirmation, MRI with endorectal coil is most accurate for local staging, particularly for excluding extraprostatic tumour extension and seminal vesicle infiltration [4, 5]. In order to increase sensitivity and specificity of the study and to reduce interobserver variation, further improvements are necessary [6, 7]. For this purpose, dynamic contrast enhanced MRI was used successfully [8–10]. It could also be shown that staging accuracy can be improved significantly by adding 3D proton MR spectroscopic imaging to the routine MRI protocol [11, 12].

An endorectal coil is routinely applied for 3D proton MR spectroscopic imaging to increase the inherent low MR spectroscopy signal [11–14]. However, patient discomfort can make the examination with an endorectal coil difficult. In addition, due to therapy-induced side effects, e.g. proctitis after radiotherapy, follow-up studies can be problematic.

Single-voxel proton MR spectroscopy examinations have been successfully performed in patients by using external surface coils [15–17]. For clinical purposes, however, 3D multivoxel techniques covering the whole prostate are mandatory for the assessment of tumour localization and extent. Recently, Kaji et al. reported that 2D MR spectroscopic imaging has comparable detection accuracy to the endorectal coil when an external surface coil is used [17]. However, for accurate diagnosis, total prostate coverage is required. This can be achieved by a 3D MR spectroscopic imaging sequence only. The aim of the present study was to evaluate the feasibility of 3D MR spectroscopic imaging with *k*-space weighted acquisition using the spine array surface coil as a receiver coil at 1.5 T in clinical routine.

## Materials and methods

### Patients

A total of 28 patients aged 41–80 years (median age 65.5 years) were examined by combined MRI and 3D proton MR spectroscopic imaging. All patients were referred consecutively to MRI for diagnostic evaluation of the prostate: 21 patients had been referred for pre-therapeutic MR imaging of biopsy-proven prostate cancer ($n$=19) or after transurethral resection of the prostate ($n$=2). Four of the 28 patients had already been treated with hormone deprivation therapy ($n$=2), seed implantation ($n$=1) or external beam radiotherapy ($n$=1). Three of the 28 patients were treated conservatively for benign prostatic hyperplasia. The median PSA level of all patients was 8.6 ng/ml (range 0.34–988 ng/ml). The mean Gleason score was six (range 3–10; median 5.5).

Patients with prostate cancer were treated by radical prostatectomy ($n$=14), external beam radiotherapy ($n$=4), brachytherapy with implantation of iodine-125 seeds ($n$=2) or hormone deprivation therapy ($n$=1). The mean time interval between MR examination and radical prostatectomy was 6.6 days (range 1–41 days). Histopathologic evaluation of prostatectomy specimens in 14 patients treated by radical prostatectomy yielded tumour confined to the prostate in nine cases (pT2a, $n$=4; pT2b, $n$=1; pT2c, $n$=4), capsular penetration (pT3a) in two cases and seminal vesicle invasion (pT3b) in three cases.

To reduce artefacts from post-bioptic haemorrhage, commonly a minimum time between biopsy and MRI/3D MRSI of 3 weeks is considered to be appropriate. All patients in our study complied with this time interval with exception of one patient (time between biopsy and MRI/3D MRSI: 16 days). No prostatic haemorrhage was observed in this particular patient.

All procedures in this study are in accordance with the standards of the responsible ethics commission and with the Declaration of Helsinki, as revised in 1983.

### MR imaging

MR examinations were performed on a 1.5 T MR whole-body scanner (Magnetom Sonata, Siemens Medical Systems, Erlangen, Germany) using the combination of standard body-phased-array and spine-phased-array surface coils positioned in front of and behind the patients' pelvis. Prior to examination all patients received 20 mg butylscopolamine Intra-Venously (Buscopan) to reduce bowel motion artefacts. All patients were examined in the supine position. The MR imaging protocol of the prostate and seminal vesicles included multiplanar T2-weighted turbo spin-echo sequences (TR/TE=7080/121 ms, turbo factor 23) and axial T1-weighted spin-echo sequences (TR/TE=450/12 ms) with a slice thickness of 3 mm, a field-of-view (FOV) of 200 mm and a matrix size of 512×256. The axial and coronal MR images were angulated along and perpendicular to the rectal wall, respectively. Total examination time of combined MRI/3D MRSI was approximate 50 min.

The MR images were evaluated by two experienced radiologists, one specialising in urological imaging. The reports were compared retrospectively with the histopathologic findings. Low intensity lesions on T2-weighted MR images within the peripheral zone of the prostate were considered as suspicious for tumour. Asymmetric bulging, irregular margin or direct extension of the lesion in the periprostatic fat was graded as capsular penetration (stage

T3a). Signs of seminal vesicle invasion included low intensity in one or both seminal vesicles (stage T3b).

### Coil selection for 3D proton MR spectroscopy

In contrast to MRI, for MR spectroscopic examinations it is not yet possible to combine multiple coil elements with the available software version on the scanner. One specific element of the spine-phased-array-coil with the best coverage of the prostate was chosen for acquisition of spectral data. The spine-array coil consists of six different loops all of which configured in ellipsoid shape (approximately 45×15 $cm^2$ in diameter). The elements are placed within the spine-phased array coil with a slight overlap to the neighbouring loop. The spatial inhomogeneity of signal reception from the prostate by the coil is not very important, since the metabolite ratios are used for evaluation.

### 3D proton MR spectroscopy sequence

The hybrid MR spectroscopic imaging (MRSI) sequence with spin-echo pre-localization and 3D spatial encoding was provided as a work-in-progress package by Siemens Medical Systems (Erlangen, Germany). The body radiofrequency coil was used for excitation and one element of the spine array coil for signal acquisition. TR and TE were optimized for the detection of citrate (TR/TE=1000/120 ms) according to literature data [14, 18]. The volume for spin excitation (volume of interest, VOI) was closely fitted to the size of the prostate based on transversal and coronal T2-weighted MR images. The field-of-view (FOV, 3D spatial encoding) was 80×80×120 $mm^3$ and was kept constant for all studies. It was slightly larger than the prostate to prevent undesired signals from periprostatic fat tissue. Sixteen acquisitions were recorded with a matrix size of 12×12×8 phase encoding steps, resulting in a nominal voxel size of 7×7×15 $mm^3$. Raw data acquisition was based on a weighted *k*-space sampling scheme. Measuring time was approximately 20 min. Raw data were multiplied with a spherically symmetric Hanning filter function in order to enhance the signal contribution from the centre of the *k*-space compared to signal from the margins. Compared to the unfiltered acquisition, the spatial response function obtained by filtering led to an enlargement of the effective voxel size by a factor of 1.78 compared to the nominal voxel size [18, 19]. On the other hand, voxel bleeding from and to distant voxels was significantly reduced. A spectral bandwidth of 1000 Hz and a vector size of 512 sample points were used and data were interpolated to a 16×16×8 matrix.

Signal suppression of lipid/water resonances was performed with spatial suppression pulses (outer volume saturation, OVS) and spectral lipid/water suppression pulses described as "MEGA" [20] or double "BASING" [14, 21–23].

Signal suppression was effective within the spectral range from 0.7 ppm to 2 ppm (lipid resonances) and from 4.0 ppm to 5.4 ppm (water resonance). Additionally, eight spatial saturation slabs were placed close to the border of the prostate for outer volume saturation (Fig. 1b). Magnetic field homogeneity (shim) was optimized in the VOI. Shimming as well as spectral fat and water signal suppression were performed automatically.

### Evaluation of 3D MRSI data

The metabolites of interest were citrate (Ci) with a strong coupled proton spin system centred at 2.6 ppm, choline-containing compounds (Cho) with methyl protons resonating at 3.2 ppm and (phosphor-)creatine (Cr) with methyl protons resonating at 3.0 ppm.

According to the histopathologic findings, the voxels and the corresponding spectra were assigned to normal glandular tissue or tumour tissue. For selected voxels, the area under the curve of the metabolite resonances was determined and the signal intensity ratio of (Cho+Cr)/Ci was calculated using a commercially available software (syngo MR 2004V; Siemens Medical, Erlangen, Germany).

Standardised data processing included the application of zero-filling to 1024 data points in the time domain, the application of a Gaussian-filter (300 ms), zero-order phase correction and automated baseline correction (polynomial; 6th order). In spectra with a poor separation of choline and creatine, the calculation of the (Cho+Cr)/Ci signal intensities ratio was performed interactively.

In addition, for selected voxel within healthy prostate tissue, signal-to-noise ratio was calculated by dividing the amplitude of the signal intensity of the Ci-Resonance by the typical noise amplitude (peak-to-peak) in the chemical shift range lacking significant signals.

The quality of the spectra was ranked independently and in consensus by two experienced radiologists into three categories: "good" was assigned to spectra with sufficient signal-to-noise ratio (>6) of the resonances of (choline+creatine) and/or citrate (Fig. 2a, b, c, d). "Acceptable" was assigned to spectra with signal-to-noise ratios between 1.5 and 6 and/or minor baseline distortions due to signal contamination from lipid resonances. "Poor" was assigned in case of considerable baseline distortions or no detectable resonances for diagnosis at all.

### Statistical evaluation

A two-sided student's *t*-test was used for analysis of metabolite ratios with respect to the differentiation of tumour and normal glandular tissue. A $P$-value $\leq 0.05$ was considered significant. For inter-observer agreement, Cohen's kappa-value was calculated. A value of $k \geq 0.8$ was considered as high inter-observer agreement.

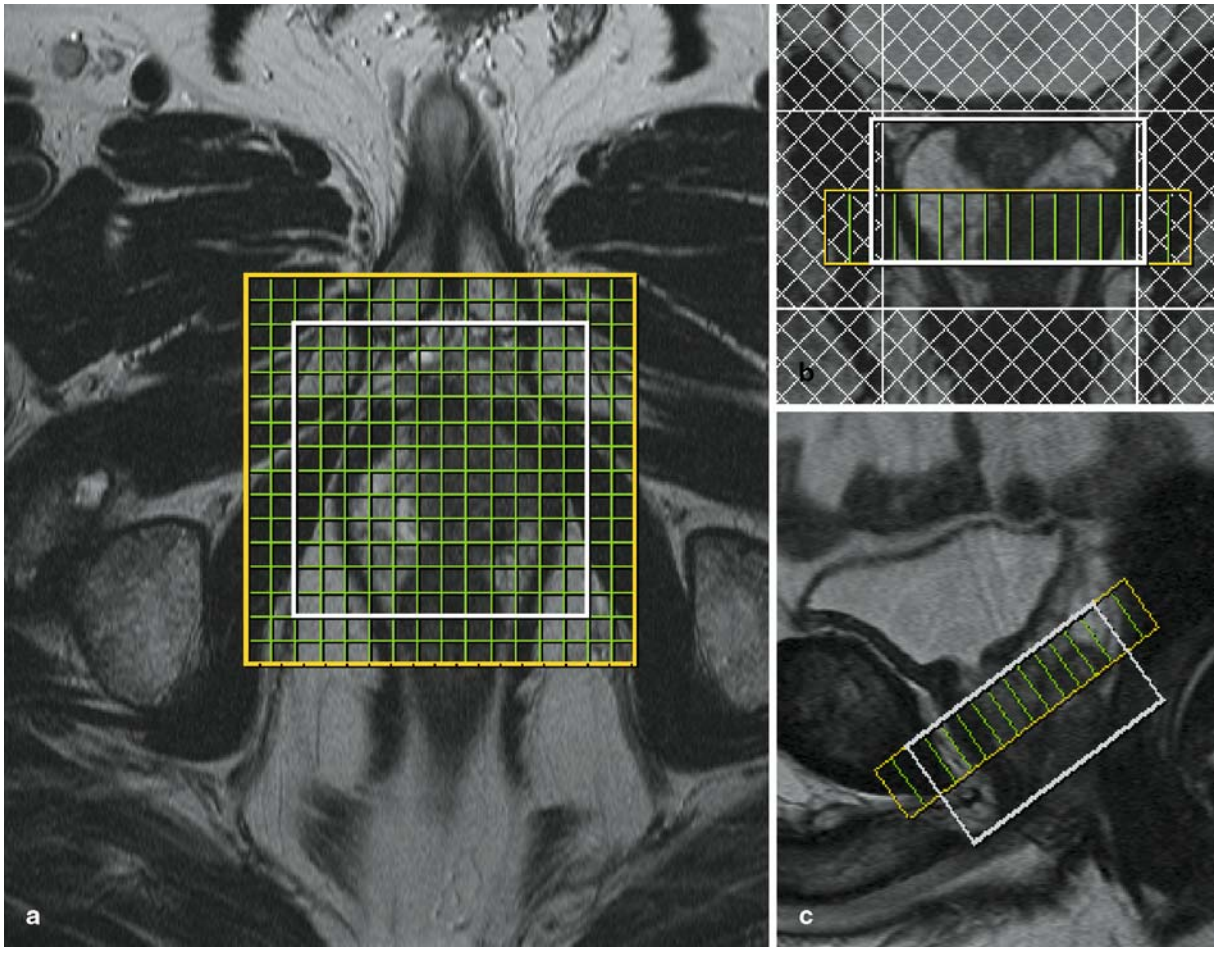


**Fig. 1** Patient with a proven adenocarcinoma of the left prostate gland (histologically confirmed by radical prostatectomy: pT3a pN1 Mo). Field-of-view (*yellow box*), area of interest (*white box*) and resulting voxel (*green grid*) for one selected slice of the 3D MR spectroscopy examination are projected on **a** axial, **b** coronal and **c** sagital T2-weighted images. Additionally, free slabs of the outer volume suppression are displayed in **b** (*white grids*). 3D MR spectroscopic imaging covered the whole prostate. Tumour tissue is characterized by a T2-weighted hypointense signal localized mainly in the left central gland

## Results

MRI reports were correct with respect to tumour staging in 9/9 pT2 and 2/2 pT3a tumours. Seminal vesicle invasion was missed in one case (correct in two out of three pT3b tumours).

### Magnetic resonance spectroscopy

There was high inter-observer agreement for the quality benchmark between the two readers ($k$>0.8). The quality (consensus read) of proton MR spectra was considered to be good in 8/28 patients (29%), acceptable in 9/28 patients (32%) and poor in 11/28 (39%) patients. All four patients who underwent therapy (after hormone deprivation $n$=2, seed-implantation $n$=1 or radiotherapy $n$=1) before 3D MR spectroscopic imaging were assigned to "poor" and of no diagnostic value (4/25 patients with proven malignancy = 16%).

The lipid suppression lead to sufficient signal suppression between 0.7 ppm and 2.0 ppm. In two cases, the signal of the citrate resonance was contaminated with signal from lipids. These examinations were classified as "poor", even though high (Cho+Cr) signal intensities were detected in tumour tissue. In 8/28 examinations, the splitting of the citrate resonance could be observed for all spectra in the VOI. Further, 8/28 cases (3D MRSI classified as "acceptable") revealed sporadic spectra with considerably baseline distortions between 2.0 ppm and 2.4 ppm. SNR for spectra with rating "good" and "acceptable" was sufficient for automated analysis. The automatic fitting routine of spectra with classification as "poor" sometimes failed. In these cases, interactive evaluation had to be performed.

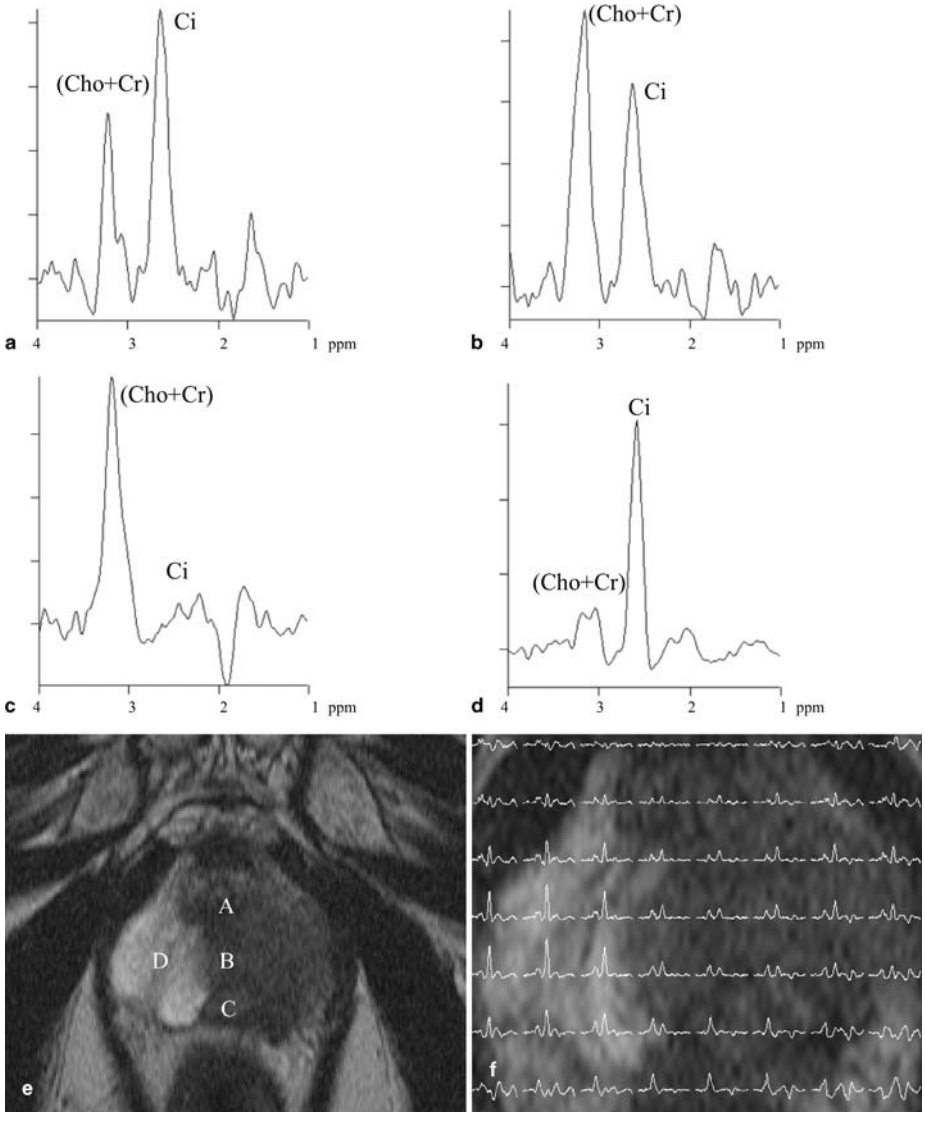


**Fig. 2** 3D MR spectroscopic imaging of the patient presented in Fig. 1. The normal tissue of the central and peripheral gland is characterized by high citrate and lower choline and creatine signal intensities (**d**). The spectra of cancer tissue showed elevated choline and decreased citrate signal intensities. Locations of spectra shown in **a–d** are given in **f**

For each patient, with the applied 3D MRSI a total number of 288 interpolated voxels were available. For determination of the signal intensities ratio of (Cho+Cr)/Ci in tumour and normal prostatic tissue/benign prostatic hyperplasia tissue, a total of 103 voxel were retrospectively evaluated according to available histopathologic data. Thirty-three voxels were placed within the proven tumours, 33 in the peripheral glands and 37 in the central glands of the patients. In prostate cancer significantly higher signal intensity ratios of (Cho+Cr)/Ci compared to tissue from the central and peripheral gland was observed ($P$=0.014) (Fig. 3, Table 1).

In 20 out of 25 patients with biopsy proven prostate cancer (80%) MR spectroscopic examinations were considered to be helpful for a better differentiation between prostate cancer and normal/benign prostatic hyperplasia tissue and improved diagnostic confidence (consensus read).

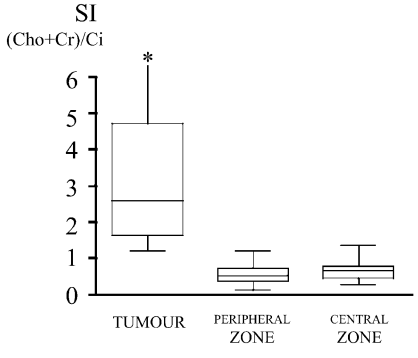


**Fig. 3** Boxplots for (Cho+Cr)/Ci signal intensities (*SI*), subdivided into tumour, central gland and peripheral zone. Figures of SI ratios are given in Table 1

**Table 1** Signal intensity ratios of (Cho+Cr)/Ci and number of evaluated voxels. Tumour tissue was characterized by significantly higher (Cho+Cr)/Ci signal intensities ratios (student's *t*-test: $P$=0.014)

| | Tumour tissue | Peripheral gland | Central gland |
|---|---|---|---|
| Minimum | 1.19 | 0.10 | 0.26 |
| Maximum | 55.58 | 1.19 | 1.35 |
| Mean | 5.37 | 0.55 | 0.64 |
| SD | 9.99 | 0.28 | 0.27 |
| Voxel | | | |
| *n* | 33 | 33 | 37 |

## Discussion

Local staging with accurate assessment of tumour extent and volume is an important prognostic factor for tumour recurrence after radical prostatectomy [12, 13]. It has been demonstrated that the diagnostic precision of a standard sextant biopsy can be achieved by the combination of MRI and 3D proton MR spectroscopic imaging with endorectal coil [24]. It was also demonstrated that also contrast enhanced dynamic MRI can improve the detection of prostate cancer [8–10]. Detailed assessment of tumour localization and extent is also important for planning minimally invasive therapeutic strategies [25–27].

3D proton MR spectroscopic imaging clearly benefits from the use of an endorectal coil. However, in patients with inflammation, anal fissures, fistulas or status post rectum extirpatio the use of endorectal coils may be difficult or even impossible. In our examinations without endorectal coil effective voxel size was enlarged and numbers of averages were increased to face the poor SNR compared to examinations of the prostate with an endorectal coil.

Spectra obtained from the patients proved to be adequate in SNR and spectral resolution in 61% for the primary detection of prostate cancer and its localisation. However, in 39% of all examinations, SNR and/or spectral resolution were insufficient. Tumour spectra showed significantly higher signal intensities ratios of (Cho+Cr)/Ci than normal prostate tissue and areas of benign prostatic hyperplasia. Based on this fact, 3D MRSI was found to improve detection of prostate cancer in 80% in cases with biopsy proven prostate cancers (20 out of 25 patients).

It has been shown that there is an overlap in the (Cho+Cr)/Ci intensities ratio between tumour and benign hyperplasia tissue. Scheidler et al. [11] considered the following rating: normal in case of a signal intensity ratios of (Cho+Cr)/Ci lower than 0.75; suspicious in case of a signal intensity ratio of (Cho+Cr)/Ci between 0.75 and 0.86, with lowered signal intensity ratio of $Ci/Ci_{(normal)}$; definitive tumour in case of signal intensity ratio of (Cho+Cr)/Ci above this threshold. However, these cut-off values are not valid for spectra acquired from periurethral voxel, where higher signal intensity ratios for (Cho+Cr)/Ci can be observed also under normal conditions [28]. In addition, voxel covering seminal vesicles may show apparently increased Cho signals.

The results of our study can be compared to the above-mentioned data because identical TR and TE values were chosen [11, 14, 29]. (Cho+Cr)/Ci signal intensities ratios were significantly higher in tumours than in normal tissue (Fig. 2c ,f, g). The non-tumourous central and peripheral regions of the gland (Fig. 2d, f, g) were not significantly different. However, compared to the data by Scheidler et al. [11] for healthy prostatic tissue, mean and maximum for (Cho+Cr)/Ci signal ratio are relatively high in the present study. This finding is probably caused by the high rate of benign prostatic hyperplasia potentially present in our patients (Fig. 3, Table 1).

With the applied 3D MRSI sequence a interpolated nominal voxel volume of 7×7×15 $mm^3$ (about 0.74 $cm^3$) was achieved. However, with bell-shaped filtering of *k*-space, an enlargement of effective voxel size is resulting. According to Scheenen et al. [18] and Pohmann et al. [19], it follows that the effective voxel size is 1.78 times the nominal size. In our study, a effective voxel size of approximately 12×12×27 $mm^3$ (approximately 3.89 $cm^3$) is resulting. The 2D MR spectroscopic imaging sequence used by Kaji et al. [17] with a standard spine array coil yielded a voxel size of 1 $cm^3$. However, data were also interpolated (to a 32×32 matrix) and effective and nominal voxel sizes were not distinguished. Using endorectal coils, Scheidler et al. and Kurhanewwicz et al. [11, 29] achieved voxel volumes between 0.24 $cm^3$ and 0.7 $cm^3$, also without distinguishing nominal and effective voxel size.

The total examination time for our combined MRI/3D MRSI is comparable to Scheidler et al. (less than 60 min) or Kurhanewicz et al. (typically 50–60 min) [11, 29]. Compared to conventional data acquisition covering the entire *k*-space with homogeneous weighting, the weighted acquisition scheme makes optimal usage of the acquisition time [18]. Of course, the weighted acquisition scheme can also be used to improve MR spectroscopic imaging with use of endorectal coils. Doing so, interpolated voxel sizes of less than 0.6×0.6×0.6 $mm^3$ with coverage of the whole prostate can be achieved within 10 min [18].

Local staging of prostate tumour is considered to be superior using endorectal coils as compared to MRI with a combination of body-phased array and spine-phased array coils [2]. It is important to note that an increased effective voxel size of about 3.89 $cm^3$ will reduce the sensitivity in the detection of prostate cancer. Regarding the potential of 3D MRSI for the detection of prostate cancer, however, no definitive relationship is indicated in the present literature between voxel size, tumour volume within the voxel and tumour grading.

Kurhanewicz et al. [29] postulated a SNR above five achieved with 3D MR spectroscopic imaging to be adequate for diagnostic purposes, particularly for the predic-

tion of extracapsular tumour extension. Based on this assumption, only 30% of our examinations were rated as good (SNR >6). Considerable baseline distortions between 2.0 ppm and 2.4 ppm were observed. These findings arise most frequently from shifting residual lipid and/or water resonances due to insufficient shimming. It should be emphasised that no resonances of Cho, Cr and Ci were detected in patients after hormone deprivation and radiotherapy/seed implantation. Müller-Lisse et al. [30] also observed markedly reduced Ci resonances in patients with hormone deprivation. However, Müller-Lisse et al. stated that performing combined MRI/3D MRSI examinations within 4 months after initiating therapy did not show reduced accuracy in localizing prostate cancer compared to nontreated patients.

## Conclusion

The results of our feasibility study indicate that combined MRI/3D MR spectroscopic imaging using the standard spine array coil instead an endorectal coil can be performed. Also the detection of prostate cancer can be improved using 3D MR spectroscopic imaging without an endorectal coil. The signal intensity ratios of citrate, choline and creatine in our study resemble those reported in the literature. This technique is therefore especially useful in patients who do not tolerate or cannot be examined with an endorectal coil. However, reduced quality of 3D MR spectroscopic imaging compared to endorectal coil examinations have to be accepted. Future work should focus on combining signals from multiple array coils for further improving signal-to-noise ratios in those spectra.

## References


1. Greenlee RT, Hill-Harmon MB, Murray T, Thun M (2001) Cancer statistics CA. Cancer J Clin 51:15–36
2. Holmberg L, Bill-Axelson A, Helgesen F, Salo JO, Folmerz P, Haggman M, Andersson SO, Spangberg A, Busch C, Nordling S, Palmgren J, Adami HO, Johansson JE, Norlen BJ, Scandinavian Prostatic Cancer Group Study Number 4 (2002) A randomized trial comparing radical prostatectomy with watchful waiting in early prostate cancer. N Engl J Med 347:781–789
3. Ikonen S, Kivisaari L, Tervahartiala P, Vehmas T, Taari K, Rannikko S (2001) Prostate MR imaging: accuracy in differentiating cancer from other prostatic disorders. Acta Radiol 42:348–354
4. Hricak H, White S, Vigneron D, Kurhanewicz J, Kosco A, Levin D, Weiss J, Narayan P, Carroll PR (1994) Carcinoma of the prostate gland: MR imaging with pelvic phased-array coils versus integrated endorectal-pelvic phased-array coils. Radiology 193:703–709
5. Jager GJ, Severens JL, Thornbury JR, de la Rosette JJ, Ruijs SH, Barentsz JO (2000) Prostate cancer staging: should MR imaging be used? A decision analytic approach. Radiology 215:445–451
6. May F, Treumann T, Dettmar P, Hartung R, Breul J (2001) Limited value of endorectal magnetic resonance imaging and transrectal ultrasonography in the staging of clinically localized prostate cancer. BJU Int 87:66–69
7. Engelbrecht MR, Jager GJ, Laheij RJ, Verbeek AL, Van Lier HJ, Barentsz JO (2002) Local staging of prostate cancer using magnetic resonance imaging: a meta-analysis. Eur Radiol 12:2294–2302
8. Schlemmer HP, Merkle J, Grobholz R, Jaeger T, Michel MS, Werner A, Rabe J, Van Kaick G (2004) Can pre-operative contrast-enhanced dynamic MR imaging for prostate cancer predict microvessel density in prostatectomy specimens? Eur Radiol 14:309–317
9. Kiessling F, Lichy M, Grobholz R, Heilmann M, Farhan N, Michel MS, Trojan L, Ederle J, Abel U, Kauczor HU, Semmler W, Delorme S (2004) Simple models improve the discrimination of prostate cancers from the peripheral gland by T1-weighted dynamic MRI. Eur Radiol 14:1793–1801
10. Rouviere O, Raudrant A, Ecochard R, Colin-Pangaud C, Pasquiou C, Bouvier R, Marechal JM, Lyonnet D (2003) Characterization of time-enhancement curves of benign and malignant prostate tissue at dynamic MR imaging. Eur Radiol 13:931–942
11. Scheidler J, Hricak H, Vigneron DB, Yu KK, Sokolov DL, Huang LR, Zaloudek CJ, Nelson SJ, Carroll PR, Kurhanewicz J (1999) Prostate cancer: localization with three-dimensional proton MR spectroscopic imaging—clinicopathological study. Radiology 213:473–480
12. Yu KK, Schneidler J, Hricak H, Vigneron CJ, Zaloudek CJ, Males RG, Neslon SJ, Carroll PR, Kurhanewiccz J (1999) Prostate cancer: prediction of extracapsular extension with endorectal MR imaging and three-dimensional proton MR spectroscopic imaging. Radiology 213:481–488
13. Coakley FV, Kurhanewicz J, Lu Y, Jones KD, Swanson MG, Chang SD, Carroll PR, Hricak H (2002) Prostate cancer tumor volume: measurement with endorectal MR and MR spectroscopic imaging. Radiology 223:91–97
14. Heerschap A, Jager G, Van der Graaf M, Barentsz J, Ruijs S (1997) Proton MR spectroscopy of the normal human prostate with an endorectal coil and a double spin-echo pulse sequence. Magn Reson Med 37:204–213
15. Schick F, Bongers H, Kurz S, Jung WI, Pfeffer M, Lutz O (1993) Localized proton MR spectroscopy of citrate in vitro and of the human prostate in vivo at 1.5 T. Magn Reson Med 29:38–43
16. Kim JK, Kim DY, Lee YH, Sung NK, Chung DS, Kim OD, Kim KB (1998) In vivo differential diagnosis of prostate cancer and benign prostatic hyperplasia: localized proton magnetic resonance spectroscopy using external-body surface coil. Magn Reson Imaging 16:1281–1288
17. Kaji Y, Wada A, Imaoka I, Matsuo M, Terachi T, Kobashi Y, Sugimura K, Fujii M, Maruyama K, Takizawa O (2002) Proton two-dimensional chemical shift imaging for evaluation of prostate cancer: external surface coil vs. endorectal surface coil. J Magn Reson Imaging 16:697–706
18. Scheenen TW, Klomp DW, Roll SA, Futterer JJ, Barentsz JO, Heerschap A (2004) Fast acquisition-weighted three-dimensional proton MR spectroscopic imaging of the human prostate. Magn Reson Med 52:80–88

19. Pohmann R, von Kienlin M (2001) Accurate phosphorus metabolite images of the human heart by 3D acquisition-weighted CSI. Magn Reson Med 45:817–826
20. Mescher M, Merkle H, Kirsch J, Garwood M, Gruetter R (1998) Simultaneous in vivo spectral editing and water suppression. NMR Biomed 11:266–272
21. Garcia-Segura J, Sanchez-Chapado M, Ibarburen C, Viano J, Angulo J, Gonzales J, Rodriguez-Vallejo J (1999) In vivo 1H MRS of diseased prostate: spectroscopic features of malignant versus benign pathology. Magn Reson Imaging 17:755–765
22. Males R, Vigneron D, Star-Lack J, Falbo S, Nelson S, Hricak H, Kurhanewicz J (2000) Clinical application of BASING and spectral/spatial water and lipid suppression pulses for prostate cancer staging and localization by in vivo 3D 1H MR spectroscopic imaging. Magn Reson Med 43:17–22
23. Star-Lack J, Nelson SJ, Kurhanewicz J, Huang LR, Vigneron DB (1997) Improved water and lipid suppression for 3D PRESS CSI using RF band selective inversion with gradient dephasing (BASING). Magn Reson Med 38:311–321
24. Wefer A-E, Hricak H, Vigneron D-B, Coakley F-V, Lu Y, Wefer J, Mueller-Lisse U, Carroll P-R, Kurhanewicz J (2000) Sextant localization of prostate cancer: comparison of sextant biopsy, magnetic resonance imaging and magnetic resonance spectroscopic imaging with step section histology. J Urol 164:400–404
25. Pirtskhalaishvili G, Hrebinko RL, Nelson JB (2001) The treatment of prostate cancer: an overview of current options. Cancer Pract 9:295–306
26. Beerlage HP, Thuroff S, Madersbacher S, Zlotta AR, Aus G, de Reijke TM, de la Rosette JJ (2000) Current status of minimally invasive treatment options for localized prostate carcinoma. Eur Urol 37:2–13
27. Schlemmer HP, Corvin S (2004) Methods for volume assessment of prostate cancer. Eur Radiol 14:597–606
28. Heerschap A, Jager GJ, Van der Graaf M, Barentsz JO, de la Rosette JJ, Oosterhof GO, Ruijter ET, Ruijs SH (1997) In vivo proton MR spectroscopy reveals altered metabolite content in malignant prostate tissue. Anticancer Res 17:1455–1460
29. Kurhanewicz J, Vigneron DB, Hricak H, Narayan P, Carroll P, Nelson SJ (1996) Three-dimensional H-1 MR spectroscopic imaging of the in situ human prostate with high (0.24–0.7 $cm^3$) spatial resolution. Radiology 198:795–805
30. Mueller-Lisse UG, Vigneron DB, Hricak H, Swanson MG, Carroll PR, Bessette A, Scheidler J, Srivastava A, Males RG, Cha I, Kurhanewicz (2001) Localized prostate cancer: effect of hormone deprivation therapy measured by using combined three-dimensional 1H MR spectroscopy and MR imaging: clinicopathologic case-controlled study. Radiology 221:380–390